Power Control of BDFRG Variable-Speed Wind Turbine System Covering All Wind Velocity Ranges

Maryam Moazen*, Rasool Kazemzadeh*‡, Mohammad-Reza Azizian*

*Renewable Energy Research Center, Electrical Engineering Faculty, Sahand University of Technology, Tabriz, Iran

(m_moazen@sut.ac.ir, r.kazemzadeh@sut.ac.ir, azizian@sut.ac.ir)

‡ Corresponding Author; Rasool Kazemzadeh, Sahand University of Technology, Tabriz, Iran, Tel: +98 41 33459362, Fax: +98 41 33444322, r.kazemzadeh@sut.ac.ir

Received: 18.02.2016 Accepted: 21.05.2016

Abstract- In this paper, a power control strategy for the brushless doubly fed reluctance generator (BDFRG) based variable-speed wind turbine system is proposed. The proposed control strategy covers all system operational regions including: maximum power point tracking (MPPT) region, constant speed region, and constant power region; whereas, the studies in the literature for the BDFRG wind turbine system are only limited to the MPPT region. For capturing maximum power from the wind in the MPPT region, a turbine power feedback based MPPT, which is a method with fast dynamic response, is used. In the constant speed region, the BDFRG speed is kept constant, and for high wind velocities in constant power region, the controller decreases the BDFRG speed to prevent the increase of the turbine power more than its rated value. In addition, a turbine power observer is proposed to obtain turbine power. The BDFRG wind turbine system model based their dynamic equations, which explained in the paper, is simulated in MATLAB/Simulink software and the performance of the proposed control strategy is studied. The simulation results verify the effectiveness of the proposed control strategy in all three operational regions as well as the acceptable performance of the turbine power observer.

Keywords Brushless doubly fed reluctance generator, variable-speed wind turbine, maximum power point tracking, ideal power curve, turbine power observer.

1. Introduction

Wind energy generation systems especially variable-speed wind turbines have attracted great interests in recent years. Their appropriate dynamic behavior and increased power capture are the most important advantages of the variable speed systems in comparison with the conventional constant speed systems [1-4]. Doubly fed induction generator (DFIG) is a commercial wind generator in variable-speed wind generation systems because of using partially-rated converter [5]. However, the DFIG has the problem of brushes and slip rings in its structure, which are unavoidable for rotor feed [6, 7].

Nowadays, the brushless doubly fed reluctance generators (BDFRG) have been proposed as a potential alternative to the existing solutions for the variable-speed wind energy generation systems [8-15]. Its brushless structure resulting in reasonable cost and high reliability of the BDFRG is the main reason of this increasing interest. On the other hand, its comparative performance with DFIG leads to consideration of the BDFRG as a suitable choice for wind generation application [16].

The BDFRG needs partially-rated converter in wind generation applications like DFIG [8-10]. In addition, its brushless structure ensures high reliability and low maintenance of the BDFRG, which is especially important for off-shore plants [17].

In literature, different methods have been proposed to control of the BDFRG. These methods can be classified into following categories: scalar control [18-21], field orientation control (FOC) [22-30], direct torque control (DTC) [25, 31-36] and direct power control (DPC) [17, 37]. A comparative analysis of these control methods can be found in [6]. In some of these researches, the BDRRG is controlled to capture maximum power from the wind [10, 20-25, 38-40]. However, the majority of the methods used to perform maximum power point tracking (MPPT) in the BDFRG system are based on the electrical torque feedback. In these

methods, electrical torque is used to calculate reference angular speed of the BDFRG; whereas, using of the turbine power as the feedback signal instead of the electrical torque in the MPPT loop, leads to faster MPPT [41]. In addition, the control zone in all above works is only limited to the MPPT region. However, for safe operation of the system, an overall control strategy is required which covers other wind turbine operational areas, constant speed and constant power regions, as well as the MPPT region [41].

In this paper, a power control strategy has been proposed for the BDFRG wind turbine system. The proposed control strategy has the advantage of covering all wind turbine system operational areas; i.e. the MPPT, constant speed and constant power regions. Moreover, the proposed MPPT method is based on the turbine power feedback which has a fast dynamic response. In addition, in high wind velocities, the turbine output power is regulated to its rated value, smoothly, by reducing the angular speed of the BDFRG. Also, for the turbine power observation, a simple observer is proposed. Furthermore, the dynamic model of the BDFRG and wind turbine is simulated in MATLAB/Simulink software and the accuracy of the proposed control strategy within the whole wind velocity range has been validated. The rest of the present paper is organized as follows: The BDFRG structure and dynamic model are expressed in Section 2. Section 3 is dedicated to the wind turbine model and other mechanical equations of the system. In Section 4, the proposed power control strategy for the BDFRG wind turbine system covering all system operational areas has been explained. The accuracy of the proposed control strategy has been checked in Section 5. Finally, a conclusion is expressed in Section 6.

2. Brushless Doubly Fed Reluctance Generator

The BDFRG has two sinusoidal distributed three-phase winding in its stator which the pole pairs and applied frequencies to these windings are different from each other. The primary winding (power winding) is directly connected to the grid and the secondary winding (control winding) is connected to the grid through a back to back converter for bi-directional power flow which is shown in Fig. 1[17].

Since the pole pairs of two stator windings are always different, so with a round rotor, there is ideally no magnetic coupling between them [9]. However, a reluctance rotor with P_r salient poles could make magnetic coupling between the primary winding with P_1 pole pairs and the secondary winding with P_2 pole pairs (supplied with angular frequencies ω_p and ω_s, respectively) by satisfying the following equations [9]:

$$P_r = P_1 + P_2 \tag{1}$$

$$\omega_r = \omega_p + \omega_s \tag{2}$$

where ω_r is the electrical angular speed of the rotor.

The space vector model of the BDFRG in an arbitrary reference frame rotating at ω can be expressed as follows [42]:

$$\boldsymbol{v_p} = R_p \boldsymbol{i_p} + \frac{d\boldsymbol{\lambda_p}}{dt} + j\omega\boldsymbol{\lambda_p} \tag{3}$$

$$\boldsymbol{v_s} = R_s \boldsymbol{i_s} + \frac{d\boldsymbol{\lambda_s}}{dt} + j(\omega_r - \omega)\boldsymbol{\lambda_s} \tag{4}$$

$$\boldsymbol{\lambda_p} = L_p \boldsymbol{i_p} + L_{ps} \boldsymbol{i_s^*} \tag{5}$$

$$\boldsymbol{\lambda_s} = L_s \boldsymbol{i_s} + L_{ps} \boldsymbol{i_p^*} \tag{6}$$

where R_p, R_s, L_p, L_s and L_{ps} are the primary resistance, the secondary resistance, the primary inductance, the secondary inductance and the primary to secondary mutual inductance, respectively. $\boldsymbol{x_p}$ and $\boldsymbol{x_s}$ are the space vectors in a reference frame rotating at ω, for the primary and secondary, respectively. It should be noted that the primary and secondary equations are expressed in two different reference frames: the primary equation, Eq. (3), in the reference frame ω and the secondary equation, Eq. (4), in the reference frame ω_r - ω. The reference frames which are used in the model are shown in Fig. 2 [12].

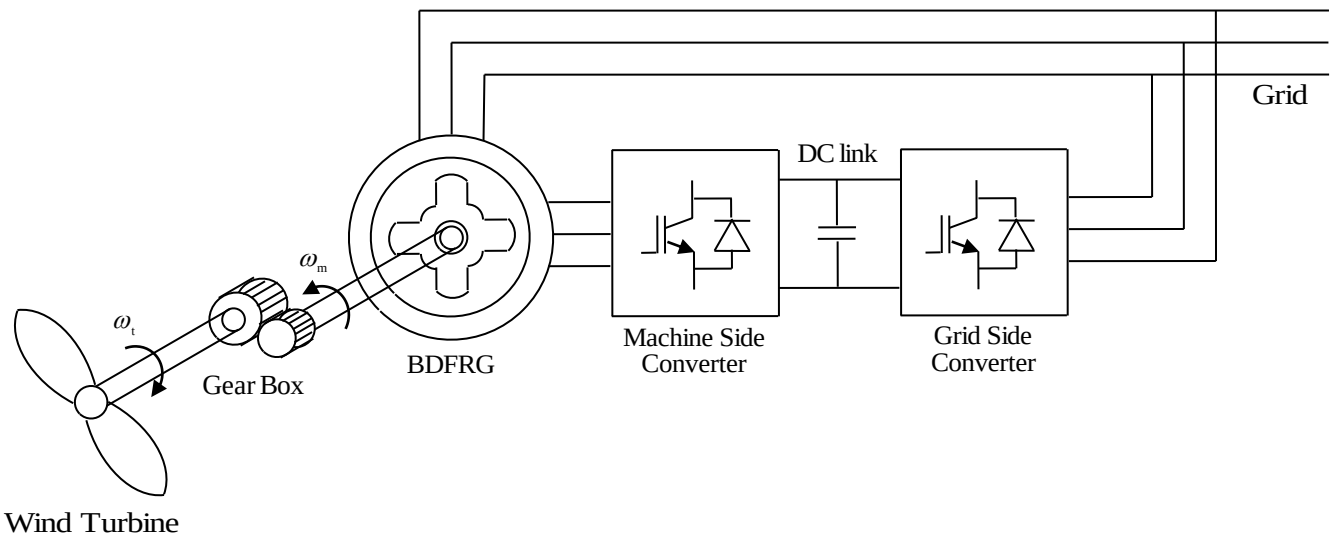

Fig. 1. The connection of the BDFRG to the grid and wind turbine.

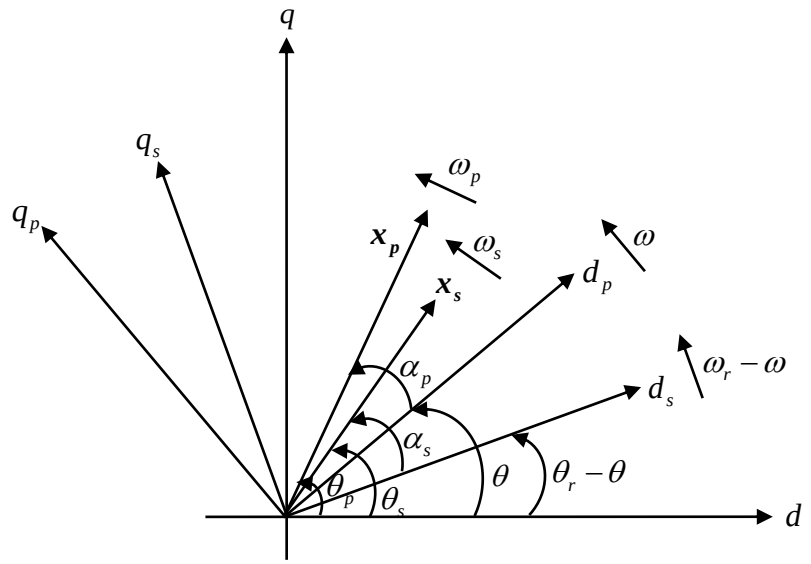

Fig. 2. The reference frames used for the BDFRG model.

In addition, The electrical torque expression of the BDFRG is [42]:

$$T_e = j\frac{3}{4}P_r L_{ps}\left(\boldsymbol{i}_p^* \boldsymbol{i}_s^* - \boldsymbol{i}_p \boldsymbol{i}_s\right) \tag{7}$$

3. Wind Turbine Model

The output power of the wind turbine, P_t, is obtained from [43]:

$$P_t = 0.5\rho\pi R^2 C_p(\lambda) v_w^3 \tag{8}$$

where ρ is the air density, R is the radius of the wind turbine blades, C_p is the power conversion coefficient and v_w is the wind velocity. C_p is a function of tip speed ratio, λ, which defined as [43]:

$$\lambda = \frac{R\omega_t}{v_w} \tag{9}$$

The turbine mechanical torque, T_t, is obtained from the turbine output power and the turbine angular speed, ω_t, as follows:

$$T_t = \frac{P_t}{\omega_t} \tag{10}$$

So, with substituting Eq. (8) and Eq. (9) into Eq. (10), T_t is obtained:

$$T_t = 0.5\rho\pi R^3 \frac{C_p(\lambda)}{\lambda} v_w^2 \tag{11}$$

With considering the gear box ratio, N, the mechanical torque, T_m, and the mechanical angular speed, ω_m, at the machine side are expressed as [43]:

$$T_m = \frac{T_t}{N} \tag{12}$$

$$\omega_m = N\omega_t \tag{13}$$

Finally, the one mass modeling of the wind turbine system is as follows [44]:

$$T_m = \left(\frac{J_t}{N^2} + J_m\right)\frac{d\omega_m}{dt} + T_e \tag{14}$$

or:

$$\frac{T_t}{N} = N\left(\frac{J_t}{N^2} + J_m\right)\frac{d\omega_t}{dt} + T_e \tag{15}$$

where J_t and J_m are the wind turbine and BDFRG inertias, respectively.

4. Control Strategy

The proposed power control strategy is based on the control of the wind turbine power to follow an ideal power curve within the whole wind velocity range. The wind turbine ideal power curve, which is shown in Fig. 3, consists of three different regions:

- Region I: the MPPT operational region; when the wind velocity varies between $v_{w\_\min}$ (the minimum wind velocity which turbine cuts in) and $v_{w\_\omega N}$ (the wind velocity which the BDFRG reaches to its maximum speed).
- Region II: the constant speed operational region; when the wind velocity varies between $v_{w\_\omega N}$ and v_{w_N} (the wind velocity which the turbine reaches to its rated power).
- Region III: the constant power operational region; when the wind velocity varies between v_{w_N} and $v_{w\_\max}$ (the maximum wind velocity which turbine cuts out).

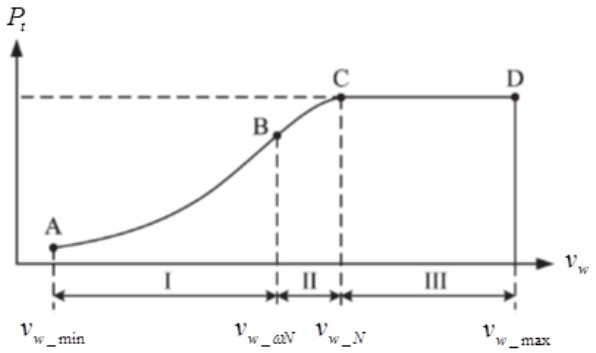

Fig. 3. The ideal power curve versus the wind velocity [41]

The block diagram of the proposed control strategy for the BDFRG wind turbine system is shown in Fig. 4. The output power of the turbine, which can be observed by a turbine power observer, P_{t_obs}, has been used to calculate the reference value for the angular speed of the BDFRG, ω_{m_ref}. The determination of the desired ω_{m_ref} in three operational regions by the proposed control strategy will be explained in the next subsections. After obtaining ω_{m_ref}, a PI controller is used to regulate ω_m to ω_{m_ref} by producing the desired reference value for the BDFRG primary active power, P_p^* (P_p^* is obtained with multiplying the output of the PI controller by ω_p/P_r). The reference values of the BDFRG primary active and reactive powers, P_p^* and Q_p^*, are applied to a lower order controller (BDFRG Power Control Block) to control the output power of the BDFRG. In fact, the BDFRG Power Control Block produces the required switching pulses for the machine side converter. It should be noted that the machine side converter controls the BDFRG active and reactive powers, and the grid side converter controls DC link voltage.

4.1. Region I: MPPT

In this operational region, the aim is to capture maximum power from the wind in different wind velocities. In the proposed MPPT method, the turbine power is used to calculate the optimal angular speed of the BDFRG.

The tip speed ratio should be equal with its optimal value, λ_{opt}, to capture maximum power from the wind turbine. Hence, when the wind velocity is changing, the BDFRG speed has to vary according to Eq. (9) in such a way that the tip speed ratio stay in its optimal value. So, in optimal operational point:

$$\lambda = \lambda_{opt} \tag{16}$$

$$C_p(\lambda) = C_{p\_\max} \tag{17}$$

where C_{p_max} is the maximum value of the power conversion coefficient. With substituting Eq. (9) into Eq. (8), and considering Eq. (16) and Eq. (17), P_t is obtained from Eq. (18) in the optimal operational point:

$$P_t = \frac{0.5\rho\pi R^5 C_{p\_\max}}{\lambda_{opt}} \omega_t^3 = k_{opt\_t}\omega_t^3 \tag{18}$$

where $k_{opt\_t} = 0.5\rho\pi R^5 C_{p\_\max} / \lambda_{opt}$. Therefore, the optimal angular speed of the turbine, ω_t^*, can be obtained as:

$$\omega_t^* = \sqrt[3]{\frac{P_t}{k_{opt\_t}}} \tag{19}$$

From Eq. (13) and Eq. (19), the optimal angular speed of the BDFRG, ω_m^*, is as follows:

$$\omega_m^* = N\sqrt[3]{\frac{P_t}{k_{opt\_t}}} \tag{20}$$

In this region, P_t is smaller than its rated value, P_{t_max}, so the Resettable PID controller in Fig. 4 is inactive and ω_{m_ref} is equal to ω_m^* which is calculated from Eq. (20) for the MPPT operation.

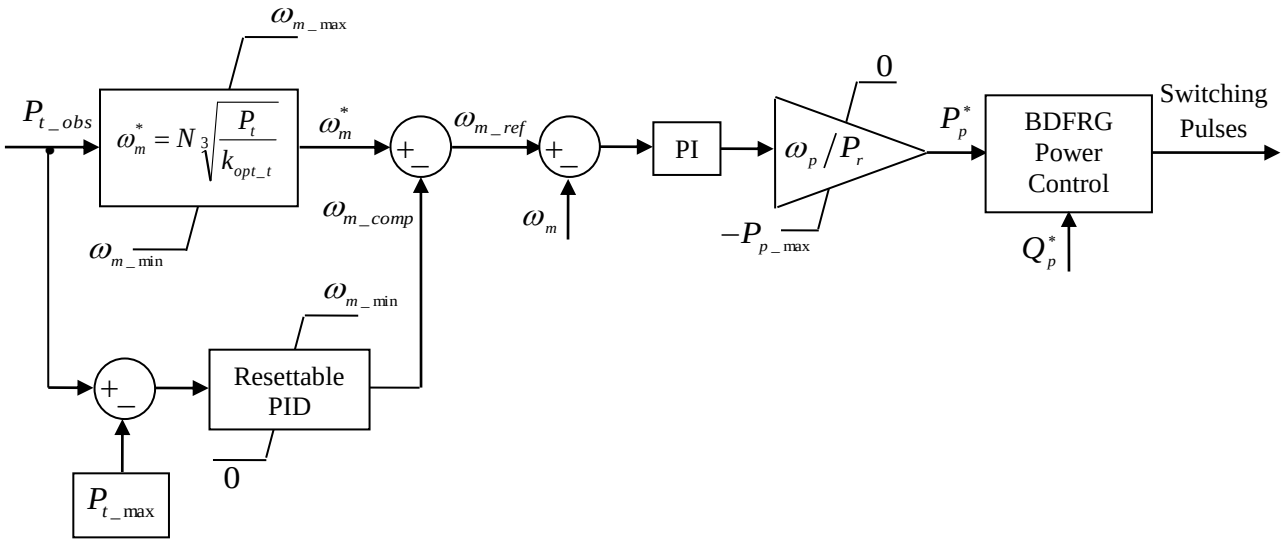

Fig. 4. The block diagram of the proposed power control strategy for the BDFRG wind turbine system within the whole wind velocity range.

4.2. Region II: Constant Speed

When the wind velocity is smaller than $v_{w\_\omega N}$, the BDFRG angular speed, ω_m, increases with the increasing of the wind velocity in the MPPT operational region. As soon as the wind velocity exceeds $v_{w\_\omega N}$, the optimal angular speed of the BDFRG, determined by Eq. (20), will reach its upper limit, $\omega_{m\_\max}$. For the wind velocities greater than $v_{w\_\omega N}$, the BDFRG angular speed remains constant, although the turbine power increases with increasing of the wind velocity. In this operational region, P_t is still smaller than $P_{t\_\max}$, and then the Resettable PID controller in Fig. 4 is inactive and ω_{m_ref} is equal to the upper limit of the ω_m^* (i.e. $\omega_{m\_\max}$).

4.3. Region III: Constant Power

When the wind velocity exceeds v_{w_N}, the power of the wind turbine reaches to $P_{t\_\max}$. If there is not any additional controller, the turbine power increases to values greater than $P_{t\_\max}$ by increasing of the wind velocity. Therefore, in this region the proposed control strategy aims to maintain the turbine power in $P_{t\_\max}$ by forcing the system to operate at lower angular speeds than $\omega_{m\_\max}$. This is performed by the Resettable PID controller which will be active when P_t exceeds $P_{t\_\max}$. The Resettable PID controller regulates P_t to $P_{t\_\max}$ by producing compensating angular speed, ω_{m_comp}. Therefore, in this region ω_{m_ref} is obtained by subtracting ω_{m_comp} from ω_m^*.

The reset option of the Resettable PID controller is triggered when the input of the controller reaches from a positive value to zero. This is necessary for clearing the output of the PID controller when the wind velocity decreases and the turbine operational region comes back from region III to region II.

4.4. Turbine Power Observer

The turbine power plays an important role in the proposed control strategy, however it cannot directly be measured and it should be observed. Fig. 5 shows a simple turbine power observer which is used in this paper to observe P_t. Eq. (14) is employed to design the turbine power observer, and rewritten as Eq. (21):

$$\frac{d\omega_m}{dt} = \frac{1}{J}\left(T_m - T_e\right) \tag{21}$$

where $J = J_t / N^2 + J_m$. On the other hand, according to Eq. (10), P_t is:

$$P_t = \omega_t T_t \tag{22}$$

Hence, with substituting Eq. (12) and Eq. (13) into Eq. (22), P_t can be obtained from multiplying ω_m by T_m:

$$P_t = \omega_m T_m \tag{23}$$

A PI controller, Eq. (21) and Eq. (23) constitute the turbine power observer structure. The PI controller regulates the observed value of the BDFRG angular speed, ω_{m_obs}, to ω_m, by producing the observed value of the BDFRG mechanical torque, T_{m_obs}. ω_{m_obs} is obtained from Eq. (21) when T_{m_obs} is used in Eq. (21) instead of T_m. Finally, the observed value of the turbine power, P_{t_obs}, is calculated from multiplying ω_{m_obs} by T_{m_obs}.

5. Simulation Results

In this section, the performance of the proposed control strategy for the BDFRG wind turbine system has been evaluated. For this purpose, the model of the BDFRG wind turbine system and the proposed control strategy are simulated in MATLAB/Simulink software. The simulated model consists of: (a) a 2 kw wind turbine, (b) a gear box, (c) a 1.5 kW BDFRG, (d) a three-phase back to back, six switch IGBT/Diode converter with 600 V DC link voltage, and (e) a balanced three-phase, 415 V, 50 Hz grid. The mechanical shaft of the BDFRG is connected to the mechanical shaft of the wind turbine through the gear box. Also, the primary winding of the BDFRG is directly connected to the grid, but its secondary winding is connected, through the back to back converter as shown in Fig. 1. The parameters of the BDFRG [13], gear box and wind turbine are reported in Table 1. Also, the parameters of the PI controller and the Resettable PID controller can be found in Table 2. The parameters of these controllers are obtained by trial and error method to achieve the best response of the test system (i.e. minimum error in BDFRG speed and turbine power, with minimum BDFRG power pulsation). In addition, Fig. 6 illustrates the $C_p - \lambda$ curve of the wind turbine. Two tests are performed to study the control system performance; first in the MPPT region only, and second in the all wind velocity areas (i.e. region I, II and III). It should be noted that the BDFRG wind turbine system startup period is not shown in the results.

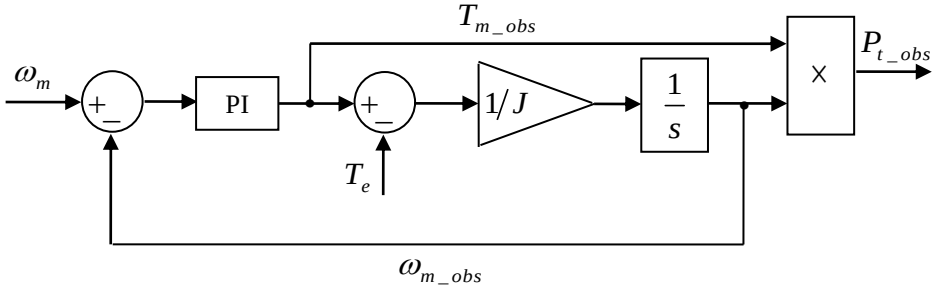

Fig. 5. The reference frames used for the BDFRG model.

Table 1. The parameters of the simulated system

Turbine Parameters		**BDFRG Parameters**	
Rated power	2 kW	Rated power	1.5 kW
Wind velocity range	3.5 – 13 m/s	Rated voltage	415 V
$v_{w\_\omega N}$	6.75 m/s	Rated speed	750 rpm
v_{w_N}	10 m/s	Maximum speed	1000 rpm
R	2 m	Poles	6/2
J_t	1.2 kg.m^2	R_p	10.7 Ω
λ_{opt}	7.9540	R_s	12.68 Ω
C_{p_max}	0.4110	L_p	0.407 H
ρ	1.225 kg/m^3	L_s	1.256 H
Gear box parameter		L_{ps}	3 H
N	3.9	J_m	0.2 kg.m^2

Table 2. The parameters of the control system

Resettable PID Parameters		**PI Parameters**	
K_p	1	K_p	10 $(P_{t\_obs} > P_{t\_max})$
K_i	0.05		50 $(P_{t\_obs} \leq P_{t\_max})$
K_d	0.01	K_i	0.1

5.1. Test 1: Control in MPPT Region

In this test, the performance of the proposed control strategy for the BDFRG wind turbine system within the MPPT region has been tested. The test is carried out when the wind velocity varies according to Fig. 7 to cover both slow and step changes.

The system outputs can be seen in Fig. 8a – Fig. 8f. Fig. 8a shows the wind turbine power and its observed value during wind velocity variation. The good agreement between the turbine power and its observed value indicates the effectiveness of the turbine power observer. Fig. 8b shows that the power conversion coefficient of the wind turbine is in its optimal value (i.e. 0.4110) during constant and slow variations of the wind velocity. Even in the step change condition, the wind turbine rapidly comes back to its optimal operational point. In Fig. 8c, the angular speed of the BDFRG is illustrated during the test condition. The active and reactive output powers of the BDFRG primary are shown in Fig. 8d. The active power tracks the generated reference value by the proposed control strategy, while the reference value of the reactive power is set to 0 VAr during the test. The electrical torque of the BDFRG is shown in Fig. 8e. The negative sign of the powers and torque indicates the power generation mode. Finally, Fig. 8f shows that the DC link voltage has been regulated to 600 V with error less than 1%.

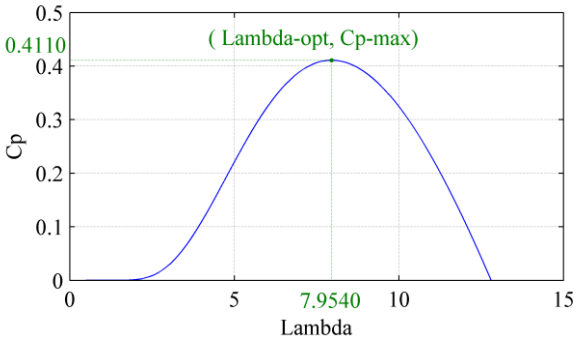

Fig. 6. The $C_p - \lambda$ curve of the wind turbine.

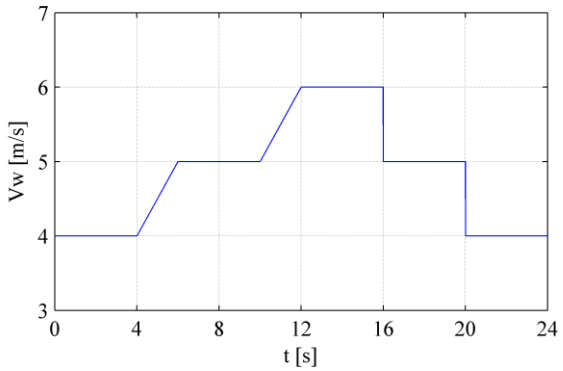

Fig. 7. The wind velocity variation curve for test condition 1.

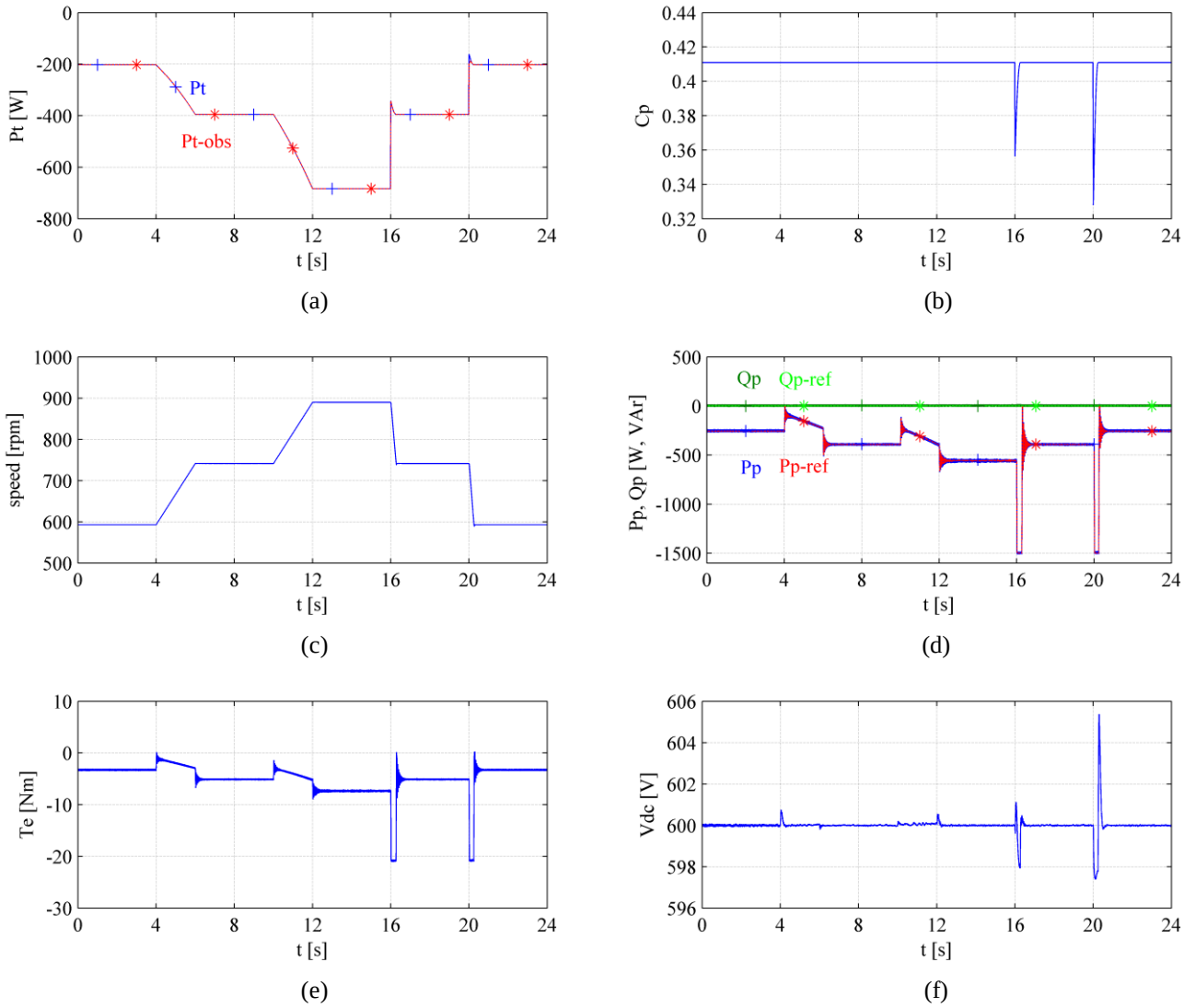

Fig. 8. The system outputs for test condition 1: (a) the wind turbine power and its observed value, (b) the power conversion coefficient of the wind turbine, (c) the angular speed of the BDFRG, (d) the active and reactive output powers of the BDFRG primary and their references values, (e) the electrical torque of the BDFRG, and (f) the DC link voltage.

5.2. Test 2: Control in All Three Regions

In this subsection, the performance of the proposed control strategy for the BDFRG wind turbine system has been verified for all three velocity regions. Fig. 9 shows the wind velocity variation during the test 2 which covering all the wind turbine operational areas in both dynamic and steady state conditions.

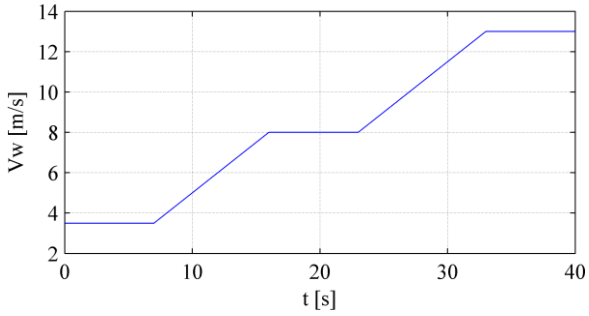

Fig. 9. The wind velocity variation curve for test condition 2.

The system outputs for test condition 2 can be seen in Fig. 10a – Fig. 10f. Fig. 10a shows the good agreement between the wind turbine power and its observed value. The power conversion coefficient of the wind turbine is shown in Fig.10b. Fig. 10c, Fig. 10d, and Fig. 10e respectively show the mechanical speed of the BDFRG, the active and reactive output powers of the BDFRG primary, and the electrical torque of the BDFRG. The negative sign of the powers and torque indicates the power generation mode. The reference value for the reactive power is 0 VAr, while the active power tracks the reference value which is generated by the proposed control strategy. The DC link voltage, which is shown in Fig. 10f, is controlled to remain in 600 V.

At first, the turbine is cut in and the wind velocity is 3.5 m/s. Between t = 0 s and t = 7 s, the wind velocity stays at 3.5 m/s, the turbine works in the MPPT region, C_p has its maximum value, and the BDFRG speed is smaller than its maximum value. By increasing the wind velocity at t = 7 s, the BDFRG speed increases until it reaches to the maximum value at $t \approx 13.5$ s; until this time, the turbine still works in

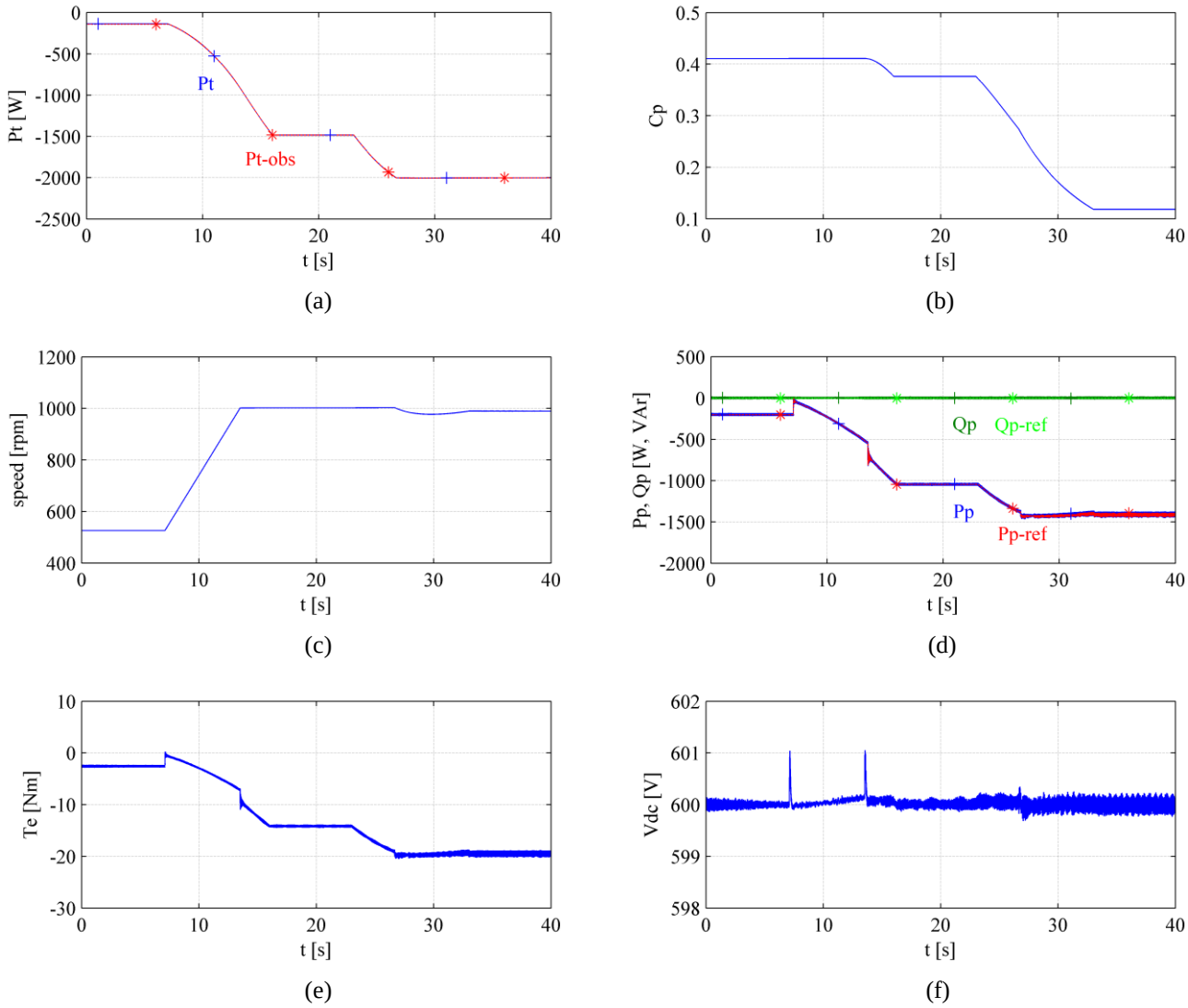

Fig. 10. The system outputs for test condition 2: (a) the wind turbine power and its observed value, (b) the power conversion coefficient of the wind turbine, (c) the angular speed of the BDFRG, (d) the active and reactive output powers of the BDFRG primary and their references values, (e) the electrical torque of the BDFRG, and (f) the DC link voltage.

the MPPT region, $C_p = C_{p\_max}$, and the captured power from the wind increases with increasing the wind velocity. As soon as the speed of the BDFRG exceeds ω_{m_max} (when the wind velocity equals to $v_{w\_\omega N}$), the operational region of the wind turbine changes from region I to region II. In region II, the controller regulates the BDFRG angular speed to ω_{m_max} and C_p decreases from its maximum value. Between $t \approx 13.5$ s and $t = 16$ s, the turbine power increases by increasing the wind velocity, and at $t = 16$ s, the wind velocity reaches to and stay at 8 m/s for the next 7 s. Again, by increasing the wind velocity at $t = 23$ s, the turbine power increases until it reaches to $P_{t\_max} = 2000$ W at $t \approx 26.65$ s (when the wind velocity reaches to $v_{w\_N} = 10$ m/s). As soon as the turbine power exceeds P_{t_max}, the operational region of the wind turbine changes from region II to region III. In region III, the controller decreases the BDFRG speed to keep the turbine power at its rated value. Between $t \approx 26.65$ s and $t = 38$ s, the turbine output power is set to 2000 W and the BDFRG speed is smaller than its maximum value (i.e. less than 1000 rpm). At $t = 24$ s, the wind velocity reaches to 13 m/s and stays constant for the rest of the test. During this time, the turbine still works in the region III. This is the maximum wind speed that the turbine can operate in, before cut out.

6. Conclusion

In this paper a power control strategy has been proposed for the BDFRG wind turbine system. The proposed strategy is based on tracking the turbine ideal power curve and covers the constant speed and constant power regions in addition to the MPPT region. The turbine power has been observed to calculate the optimal value of the BDFRG speed in the MPPT region. Also, a Resettable PID controller has been used to limit the turbine power to its rated value. The simulation results firstly verified the performance of the turbine power observer. Furthermore, the effectiveness of the proposed control strategy in all three regions is demonstrated by forcing the system to work at the optimal point in the MPPT region, at the maximum speed in the constant speed region, and at the rated power in the constant power region.

The advantages of the proposed control strategy are covering all system operational areas, using fast MPPT as well as having simple controller structure. In addition, the controller ensures safe operation of the BDFRG wind turbine system because of preventing the turbine power and the BDFRG speed exceed from their maximum values.

References

[1] S. Heier, Grid integration of wind energy conversion systems: Wiley, 1998.

[2] M. Mansour, M. Mansouri, and M. Mmimouni, "Study and control of a variable-speed wind-energy system connected to the grid," International Journal of Renewable Energy Research, vol. 1, no. 2, pp. 96-104, 2011.

[3] M. Abdelhafidh, M. Mahmoudi, L. Nezli, and O. Bouchhida, "Modeling and control of a wind power conversion system based on the double-fed asynchronous generator," International Journal of Renewable Energy Research, vol. 2, no. 2, pp. 300-306, 2012.

[4] N. Harrabi, M. Souissi, A. Aitouche, and M. Chabaane, "Intelligent control of wind conversion system based on PMSG using TS fuzzy scheme," International Journal of Renewable Energy Research, vol. 5, no. 4, pp. 952-960, 2015.

[5] V.-T. Phan, T. Logenthiran, W. L. Woo, D. Atkinson, and V. Pickert, "Analysis and compensation of voltage unbalance of a DFIG using predictive rotor current control," International Journal of Electrical Power & Energy Systems, vol. 75, pp. 8-18, 2016.

[6] M. Jovanovic, "Sensored and sensorless speed control methods for brushless doubly fed reluctance motors," IET Electric Power Applications, vol. 3, no. 6, pp. 503-513, 2009.

[7] R. Cardenas, R. Pena, P. Wheeler, J. Clare, A. Munoz, and A. Sureda, "Control of a wind generation system based on a brushless doubly-fed induction generator fed by a matrix converter," Electric Power Systems Research, vol. 103, pp. 49-60, 2013.

[8] R. E. Betz and M. G. Jovanovic, "The brushless doubly fed reluctance machine and the synchronous reluctance machine-a comparison," IEEE Transactions on Industry Applications, vol. 36, no. 4, pp. 1103-1110, 2000.

[9] R. E. Betz and M. G. Jovanovic, "Theoretical analysis of control properties for the brushless doubly fed reluctance machine," IEEE Transactions on Energy Conversion, vol. 17, no. 3, pp. 332-339, 2002.

[10] M. G. Jovanovic, R. E. Betz, and Y. Jian, "The use of doubly fed reluctance machines for large pumps and wind turbines," IEEE Transactions on Industry Applications, vol. 38, no. 6, pp. 1508-1516, 2002.

[11] W. Fengxiang, Z. Fengge, and X. Longya, "Parameter and performance comparison of doubly fed brushless machine with cage and reluctance rotors," IEEE Transactions on Industry Applications, vol. 38, no. 5, pp. 1237-1243, 2002.

[12] R. E. Betz and M. G. Jovanovic, "Introduction to the space vector modeling of the brushless doubly fed reluctance machine," Electric Power Components & Systems, vol. 31, no. 8, pp. 729-755, 2003.

[13] M. G. Jovanovic, Y. Jian, and E. Levi, "Encoderless direct torque controller for limited speed range applications of brushless doubly fed reluctance motors," IEEE Transactions on Industry Applications, vol. 42, no. 3, pp. 712-722, 2006.

[14] D. G. Dorrell and M. Jovanovic, "On the possibilities of using a brushless doubly-fed reluctance generator in a 2 MW wind turbine," 2008 IEEE Industry Applications Society Annual Meeting, Edmonton, Alta, pp. 1-8, 5-9 October 2008.

[15] M. Moazen, R. Kazemzadeh, and M. R. Azizian, "Mathematical modeling and analysis of brushless doubly fed reluctance generator under unbalanced grid voltage condition, " International Journal of Electrical Power & Energy Systems, vol. 83, pp. 547-559, 2016.

[16] J. Poza, E. Oyarbide, D. Roye, and M. Rodriguez, "Unified reference frame dq model of the brushless doubly fed machine," IEE Proceedings: Electric Power Applications, vol. 153, no. 5, pp. 726-734, 2006.

[17] H. Chaal and M. Jovanovic, "Power control of brushless doubly-fed reluctance drive and generator systems," Renewable Energy, vol. 37, no. 1, pp. 419-425, 2012.

[18] M. G. Jovanovic, R. E. Betz, Y. Jian, and E. Levi, "Aspects of vector and scalar control of brushless doubly fed reluctance machines," 4th IEEE International Conference on Power Electronics and Drive Systems pp. 461-467, 22-25 October 2001.

[19] M. Hassan and M. Jovanovic, "Improved scalar control using flexible DC-Link voltage in brushless doubly-fed reluctance machines for wind applications," 2nd International Symposium on Environment Friendly Energies and Applications, pp. 482-487, 25-27 June 2012.

[20] M. G. Mousa, S. M. Allam, and E. M. Rashad, "A sensorless scalar-control strategy for maximum power tracking of a grid-connected wind-driven Brushless Doubly-Fed Reluctance Generator," 4th International Conference on Electric Power and Energy Conversion Systems, Sharjah, United Arab Emirates, pp. 1-6, 24-26 November 2015.

[21] M. G. Mousa, S. M. Allam, and E. M. Rashad, "Maximum power tracking of a grid-connected wind-driven brushless doubly-fed reluctance generator using scalar control," 2015 IEEE GCC Conference and Exhibition, Muscat, pp. 1-6, 1-4 February 2015.

[22] M. G. Mousa, S. M. Allam, and E. M. Rashad, "Vector control strategy for maximum wind-power extraction of a grid-connected wind-driven Brushless Doubly-Fed

Reluctance Generator," 4th International Conference on Electric Power and Energy Conversion Systems, Sharjah, United Arab Emirates, pp. 1-6, 24-26 November 2015.

[23] M. Jovanovic, S. Ademi, and J. Obichere, "Comparisons of vector control algorithms for doubly-fed reluctance wind generators," Transactions on Engineering Technologies, pp. 85-99, 2015.

[24] S. Ademi, M. G. Jovanovic, and M. Hasan, "Control of brushless doubly-fed reluctance generators for wind energy conversion systems," IEEE Transactions on Energy Conversion, vol. 30, no. 2, pp. 596-604, 2015.

[25] S. Ademi and M. Jovanovic, "Robust vector controllers for brushless doubly-fed wind turbine generators," 2014 IEEE International Energy Conference, Cavtat, pp. 1-8, 13-16 May 2014.

[26] S. Ademi and M. Jovanovic, "Control of doubly-fed reluctance generators for wind power applications," Renewable Energy, vol. 85, pp. 171-180, 2016.

[27] X. Longya, L. Zhen, and K. Eel-Hwan, "Field-orientation control of a doubly excited brushless reluctance machine," IEEE Transactions on Industry Applications, vol. 34, no. 1, pp. 148-155, 1998.

[28] S. Ademi and M. Jovanovic, "Vector control strategies for brushless doubly-fed reluctance wind generators," 2nd International Symposium on Environment Friendly Energies and Applications, Newcastle upon Tyne, pp. 44-49, 25-27 June 2012.

[29] S. Ademi and M. Jovanovic, "Vector control methods for brushless doubly-fed reluctance machines," IEEE Transactions on Industrial Electronics, vol. 62, no. 1, pp. 96-104, 2015.

[30] S. Ademi and M. Jovanovic, "High-efficiency control of brushless doubly-fed machines for wind turbines and pump drives," Energy Conversion and Management, vol. 81, no. 0, pp. 120-132, 2014.

[31] M. Jovanovic, J. Yu, and E. Levi, "Direct torque control of brushless doubly fed reluctance machines," Electric Power Components & Systems, vol. 32, no. 10, pp. 941-958, 2004.

[32] H. Chaal and M. Jovanovic, "A new sensorless torque and reactive power controller for doubly-fed machines," 2010 International Conference on Electrical Machines, Rome, pp. 1-6, 6-8 September 2010.

[33] H. Chaal and M. Jovanovic, "Toward a generic torque and reactive power controller for doubly fed machines," IEEE Transactions on Power Electronics, vol. 27, no. 1, pp. 113-121, 2012.

[34] H. Chaal and M. Jovanovic, "Practical implementation of sensorless torque and reactive power control of doubly fed machines," IEEE Transactions on Industrial Electronics, vol. 59, no. 6, pp. 2645-2653, 2012.

[35] W. K. Song and D. G. Dorrell, "Improved direct torque control method of brushless doubly-fed reluctance machines for wind turbine," 2013 IEEE International Symposium on Industrial Electronics, Taipei, Taiwan, pp. 1-5, 28-31 May 2013.

[36] W. K. Song and D. G. Dorrell, "Implementation of improved direct torque control method of brushless doubly-fed reluctance machines for wind turbine," 2014 IEEE International Conference on Industrial Technology, Busan, pp. 509-513, 26 February - 1 March 2014.

[37] H. Chaal and M. Jovanovic, "Direct power control of brushless doubly-fed reluctance machines," 5th IET International Conference on Power Electronics, Machines and Drives, Brighton, UK, pp. 1-6, 19-21 April 2010.

[38] X. Longya and Y. Tang, "A novel wind-power generating system using field orientation controlled doubly-excited brushless reluctance machine," 1992 IEEE Industry Applications Society Annual Meeting, pp. 408-413, 4-9 Oct 1992.

[39] F. Valenciaga and P. F. Puleston, "Variable structure control of a wind energy conversion system based on a brushless doubly fed reluctance generator," IEEE Transactions on Energy Conversion, vol. 22, no. 2, pp. 499-506, 2007.

[40] F. Valenciaga and C. A. Evangelista, "2-sliding active and reactive power control of a wind energy conversion system," IET Control Theory & Applications, vol. 4, no. 11, pp. 2479-2490, 2010.

[41] C. Jiawei, C. Jie, and G. Chunying, "New overall power control strategy for variable-speed fixed-pitch wind turbines within the whole wind velocity range," IEEE Transactions on Industrial Electronics, vol. 60, no. 7, pp. 2652-2660, 2013.

[42] R. Betz and M. Jovanovic, Introduction to brushless doubly fed reluctance machines-the basic equations, Tech. Rep., Dept. Elec. Energy Conversion, Aalborg University, Denmark, 1998.

[43] G. Abad, J. Lopez, M. Rodríguez, L. Marroyo, and G. Iwanski, Doubly fed induction machine: modeling and control for wind energy generation: John Wiley & Sons, 2011.

[44] M. Monfared, H. Madadi Kojabadi, and H. Rastegar, "Static and dynamic wind turbine simulator using a converter controlled dc motor," Renewable Energy, vol. 33, no. 5, pp. 906-913, 2008.